ARTICLE

# Influence of Doped Ions on Persistent Luminescence Materials: a Review①

ZHANG Liu-Wei SHEN Rui-Chen
TAN Jie② YUAN Quan②
(*Institute of Chemical Biology and Nanomedicine, State Key Laboratory of Chemo/Biosensing and Chemometrics, College of Chemistry and Chemical Engineering, Hunan University, Changsha* 410082, *China*)

**ABSTRACT** Persistent luminescence materials (PLMs) are potential luminescent materials which can remain emitting light after stopping the excitation. PLMs can avoid the autofluorescence of biological tissues, and play an important role in biosensing, targeted imaging and other fields. However, the applications of PLMs are often restricted by their weak persistent luminescence and short decay time after excitation. Doped ions will directly affect the luminescence centers and trap levels of PLMs, thereby leading to great differences in the optical performance of PLMs. Given this, the selection of doped ions to improve the optical performance of PLMs has become a fascinating research direction in recent years. At present, the published reviews mostly focus on the surface modifications and applications of PLMs. However, the influence of doped ions on the structure and optical performance of PLMs is seldom summarized. In this review, the influence of doped ions on the structure and optical performance of PLMs is introduced from three aspects: the type of doped ions, the number of types of doped ions, and the content of doped ions. Furthermore, we highlight recent achievements and mechanisms in the development of PLMs. Finally, we also propose and discuss the future opportunities and current challenges of ion-doped PLMs.

**Keywords: persistent luminescence, doped ions, structure and optical performance;**
**DOI: 10.14102/j.cnki.0254-5861.2011-3237**

## 1 INTRODUCTION

Persistent luminescence materials (PLMs) can absorb excitation energy and continue to emit light after the excitation is stopped[1-7]. In ancient China, natural minerals with luminous properties were made into luminous cups and night pearls. In 1866, Sidot et al. first prepared the sulfide PLMs ZnS:$Cu^{2+}$, making PLMs enter the vision of researchers[8]. In 1968, Pailil et al. observed the persistent luminescence of $SrAl_2O_4$:$Eu^{2+}$, pushing the researches of PLMs into a new stage[9, 10]. Subsequently, Matsuzawa et al. found that the phosphorescence intensity and phosphorescence time of $SrAl_2O_4$:$Eu^{2+}$, $Dy^{3+}$ phosphors were more than ten times those of early PLMs[11]. Since then, many PLMs have been developed and widely used in transportation, military facilities, biosensing and other fields[12-15].

The persistent luminescence inherence makes PLMs proper candidates in material applications. Given this, many researchers are devoted to finding ways to improve the phosphorescence intensity and phosphorescence time of PLMs. The introduction of doped ions provides a possibility to improve the optical performance of PLMs[16-23]. For example, Yamamoto et al. discovered that the phosphorescence intensity and phosphorescence time of the materials were improved after introducing $Dy^{3+}$ ion into $SrAl_2O_4$:$Eu^{2+}$[11]. Liu et al. enhanced the phosphorescence intensity and prolonged the phosphorescence time exceeding 13 hours by adjusting the contents of $Nd^{3+}$ ion in $Zn_2Ga_{3-x-y}Ge_{0.75}O_8$:$Cr_x$, $Nd_y$[24]. Studying the mechanisms of ion doping to enhance the optical performance of PLMs can help design PLMs with stronger phosphorescence intensity and longer phosphorescence time, thereby expanding the appli-

Received 26 April 2021; accepted 2 July 2021
① This research was supported by the Natural Science Foundation of Hunan Province, China (Nos. 2020JJ4173 and 2020JJ5038)
② Corresponding authors. Yuan Quan, professor, majoring in the synthesis of nanomaterials and related biological applications.
Tan Jie, associate professor, majoring in the design of chemically modified nucleic acids for biosensing. E-mails: yuanquan@whu.edu.cn and tanjie0416@hnu.edu.cn

cations of PLMs.

Recently, reviews focus on synthesis methods, persistent luminescence mechanisms and applications of PLMs have been published. Li et al. systematically summarized the synthesis techniques, persistent luminescence mechanisms, characterizations and applications of PLMs[9]. Wang et al. summarized the persistent luminescence mechanisms, synthesis methods and biomedical applications of PLMs[25]. Singh et al. outlined the surface modifications, bioimaging applications of PLMs, and future research directions[26]. Doped ions play a vital role in improving the optical performance of PLMs. However, the influence of doped ions on the structure and optical performance of PLMs is seldom summarized. In this review, we mainly focus on how the optical performance of PLMs is affected by the type of doped ions, the number of types of doped ions, and the content of doped ions. Furthermore, the opportunities and challenges of PLMs in ion doping are also presented.

## 2 INFLUENCE OF DOPED IONS ON THE STRUCTURE AND OPTICAL PERFORMANCE OF PLMs

With the introduction of doped ions, different energy levels are produced in PLMs, resulting in different structures and optical performance. Herein, we classify and discuss how doped ions affect the structure and optical performance of PLMs based on the number of types of doped ions, the type of doped ions and the content of doped ions. To better demonstrate the influence of doped ions on PLMs, a summary of the main influence of doped ions on some common ion-doped PLMs is shown in Table 1.

**Table 1. Details of Host, Emitter, Co-dopants, Emission Region and Afterglow Decay of PLMs**

| Host | Emitter | Co-dopants | Emission region | Afterglow decay | Ref. |
|---|---|---|---|---|---|
| $SrAl_2O_4$ | $Eu^{2+}$ | | 450～700 nm | > 2 h | 4 |
| $GdAlO_3$ | $Mn^{2+}$ | $Ge^{4+}$ | 600～840 nm | > 1200 s | 64 |
| $Y_3Al_{5-x}Ga_xO_{12}$ ($x$ = 0～4) | $Ce^{3+}$ | $Bi^{3+}$ | 505 nm | 54～68 min | 67 |
| $ZnGa_2O_4$ | $B^{3+}$ | | 502,695 nm | 600 s | 18 |
| $Zn_{1.25}Ga_{1.5}Ge_{0.25}O_4$ | $Cr^{3+}$ | $Yb^{3+}$, $Er^{3+}$ | 650～850 nm | > 480 h | 23 |
| $Li_2ZnGeO_4$ | $Mn^{2+}$ | | 550～800 nm | > 960 h | 62 |
| $MgGeO_3$ | $Mn^{2+}$ | $Bi^{3+}$ | 680 nm | 100 min | 68 |
| $Y_3Sc_2Ga_3O_{12}$ | $Ce^{3+}$ | | 500 nm | 100 min | 69 |
| $CaMgSi_2O_6$ | $Eu^{2+}$ | $Dy^{3+}$, $Mn^{2+}$ | 468, 600, 670 nm | > 600s | 66 |
| $Ca_9Bi(PO_4)_7$ | $Ce^{3+}$ | $Tb^{3+}$, $Mn^{2+}$ | 300～500 nm | 5 h | 70 |
| $Ca_2BO_3Cl$ | $Eu^{2+}$ | $Dy^{3+}$ | 580 nm | 48 h | 71 |
| $Gd_2O_2S$ | $Eu^{3+}$ | $Ti^{4+}$, $Mg^{2+}$ | 580～720 nm | 120 s | 20 |
| $Lu_2O_3$ | $Tb^{3+}$ | $Ca^{2+}$ | 543 nm | 20～30 h | 72 |
| $KY_3F_{10}$ | $Tb^{3+}$ | | 542 nm | 108 s | 73 |
| AlN | $Mn^{2+}$ | | 570～700 nm | 1 h | 74 |

### 2. 1 Influence of doped ions type on the structure and optical performance of PLMs

Due to the difference in the atomic structure and energy levels, various doped ions have different effects on the structure and optical performance of PLMs. Thus, the relationship between the type of doped ions and the structure and optical performance of PLMs is introduced in this section.

#### 2. 1. 1 $Cr^{3+}$-doped PLMs

$Cr^{3+}$ ion is usually introduced into PLMs to obtain red or near-infrared persistent luminescence resulting from its unique electronic transitions. Among them, $Cr^{3+}$-doped $ZnGa_2O_4$ is one of the research hotspots in PLMs. The $ZnGa_2O_4$ crystal exhibits a cubic spinel structure, in which the $Zn^{2+}$ ion occupies the A-sites of the tetrahedron, and the $Ga^{3+}$ ion the B-sites of the octahedron[27, 28]. $Cr^{3+}$ ion tends to replace $Ga^{3+}$ ion in the distorted octahedral coordination for the reason that $Cr^{3+}$ ion has the same valence electron and ion radius as $Ga^{3+}$ ion, which makes the $Cr^{3+}$-doped $ZnGa_2O_4$ materials produce strong near-infrared phosphorescence at 696 nm[2, 29, 30]. Hao et al. found that the $Cr^{3+}$-doped $ZnGa_2O_4$ exhibits excellent optical performance, which can maintain phosphorescence for 10 hours after stopping the ultraviolet light irradiation[31]. Moreover, the author observed that the excitation spectrum of $Cr^{3+}$-doped $ZnGa_2O_4$ has three excitation bands of 250～350, 350～487, and 487～650 nm, which are caused by the host excitation band of $ZnGa_2O_4$, the charge transfer between $ZnGa_2O_4$ and $Cr^{3+}$ ion, and the

electronic transitions of $Cr^{3+}$ ion, respectively. Based on previous researches, Yan et al. further comprehensively studied the persistent luminescence mechanism of $Zn_{2.94}Ga_{1.96}Ge_2O_{10}:Cr^{3+}$[19]. As shown in Fig. 1, after the $Zn_{2.94}Ga_{1.96}Ge_2O_{10}$ absorbs incident photons, the electrons of $Zn_{2.94}Ga_{1.96}Ge_2O_{10}$ move to the conduction band and are trapped by native defects by means of nonradiative relaxation. When the ultraviolet light excitation is finished, the combination of holes and electrons released by native defects produces short phosphorescence. Since the absorption spectrum of $Cr^{3+}$ ion fully overlaps with the emission spectrum of $Zn_{2.94}Ga_{1.96}Ge_2O_{10}$, the energy absorbed by $Zn_{2.94}Ga_{1.96}Ge_2O_{10}$ is transferred to $Cr^{3+}$ ion by means of nonradiative energy[32]. The continuous energy transfer causes the electrons of $Cr^{3+}$ ion to transform into three different excited states. Then, the electrons are trapped by the shallow electron traps or deep electron traps by means of nonradiative relaxation[33]. At the same time, the electron ($t^2e$) fills the energy-matched traps in the form of $^4T_1$ and $^4T_2$ through the tunneling process. When the continuous energy transfer is stopped, the electron traps release the electrons which recombine with $Cr^{3+}$ ion, thereby producing a strong or ultra-long phosphorescence[19].

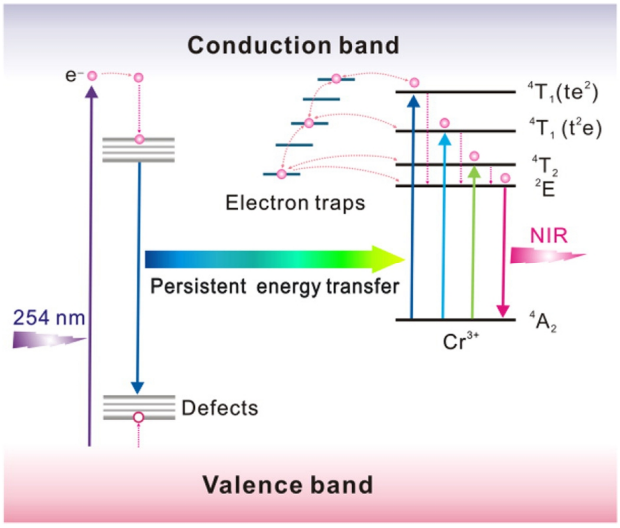


**Fig. 1. Persistent energy transfer mechanism of $Cr^{3+}$-doped $ZnGa_2O_4$ materials**

### 2. 1. 2 $Mn^{2+}$-doped PLMs

$Mn^{2+}$ ion has a typical $3d^5$ electronic configuration. The energy transitions of $Mn^{2+}$ ions are quite sensitive to the ligand/crystal field due to the participation of the *d* shell. $Mn^{2+}$ ions surrounded by anions can have different geometric structures, such as linear, octahedron, spherical, tetrahedron, or square plane. The environment of $Mn^{2+}$ ion at different crystal fields leads to different emission energy distributions and produces an emission band of 450～750 nm. For example, tetrahedral coordination of $Mn^{2+}$ ion produces green emission[34], while octahedral coordination of $Mn^{2+}$ ion produces orange to red emission[35, 36]. Tan et al. researched the size, crystal structure and optical performance of $Mn^{2+}$-doped $ZnGa_2O_4$ with a typical rod-shaped structure in different environments[21]. The size of $Mn^{2+}$-doped $ZnGa_2O_4$ rapidly decreases as the pH increases from 6 to 7.5. In comparison, when the pH further increases to 9.5, the size of the $Mn^{2+}$-doped $ZnGa_2O_4$ materials slightly increases to 80 nm. The detailed crystal structure of the $Mn^{2+}$-doped $ZnGa_2O_4$ shows that the materials have lattice fringe (110) parallel to the direction of the crystal rod and lattice fringe (113) at an angle of 66° to the direction of the crystal rod[37]. Their interplanar spacing is 0.71 and 0.29 nm, indicating that the $Mn^{2+}$-doped $ZnGa_2O_4$ grows along the *c* axis[38]. The optical performance of $ZnGa_2O_4:Mn^{2+}$ materials was further researched by researchers[39]. The photoluminescence spectrum of $Mn^{2+}$-doped $ZnGa_2O_4$ materials shows that two emission peaks are detected at 450 and 480 nm, which are resulted from the native defects, for example, interstitial Zn and oxygen vacancies (Fig. 2a). When the pH is below 7.0, the intrinsic luminescence of the materials and the emission of $Mn^{2+}$ ions have a serious overlap. As the pH increases, the intrinsic luminescence intensity gradually decreases, and the emission band intensity of the $Mn^{2+}$ ion increases. The intrinsic luminescence almost disappears and is dominated by the green emission band of $Mn^{2+}$ when the pH increases to 9.5. In this case, the phosphorescence time of $Mn^{2+}$-doped $ZnGa_2O_4$ materials exhibits more than 100 s (Fig. 2b).

According to the above results, a possible persistent luminescence mechanism of $Mn^{2+}$-doped $ZnGa_2O_4$ materials is proposed (Fig. 2c)[40, 41]. The excited electrons and holes produced under ultraviolet light excitation are trapped by electron traps and hole traps, respectively[42]. Then, some electrons get away from the electron traps under thermal stimulation and transfer to native defects, thereby resulting in the formation of emission peaks from $ZnGa_2O_4$ materials[43]. The other part of the electrons escape and transfer to the excitation level of the $Mn^{2+}$ ion[44]. Subsequently, the recombination of holes and electrons causes $Mn^{2+}$ ion to emit green light[45].

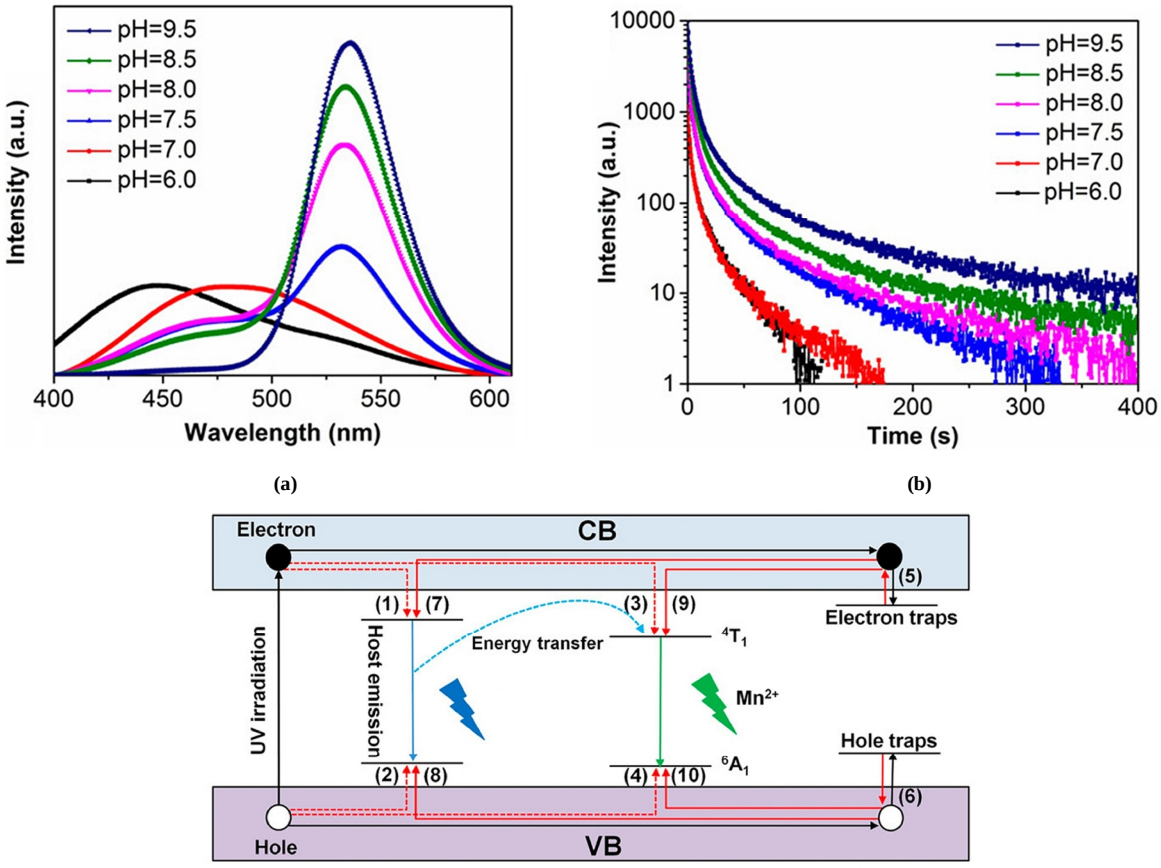


**Fig. 2. (a) Photoluminescence spectrum, (b) phosphorescence decay curve, (c) persistent energy transfer mechanism of $ZnGa_2O_4$:$Mn^{2+}$ materials**

### 2. 1. 3 $Eu^{2+}$-doped PLMs

$Eu^{2+}$ ion is a common doped ion in PLMs. The introduction of $Eu^{2+}$ ion usually produces yellow, orange and red emissions for the reason that the crystal field reduces the emission energy of $4f^65d^1$ electron configuration of $Eu^{2+}$ ion[46]. Yang et al. researched the structure and optical performance of $Eu^{2+}$-doped $SrAl_2O_4$ materials[4]. It is found that the crystal phase of the $Eu^{2+}$-doped $SrAl_2O_4$ materials corresponds to the standard pattern, indicating that the structure of the $SrAl_2O_4$ materials has not obviously changed after the introduction of $Eu^{2+}$ ion. Moreover, $Eu^{2+}$-doped $SrAl_2O_4$ shows a strong emission band of 450～700 nm and exhibits a phosphorescence time that exceeds 2 hours. Considering the structure and characteristics of $SrAl_2O_4$:$Eu^{2+}$, a possible persistent luminescence mechanism of $SrAl_2O_4$:$Eu^{2+}$ is deduced. The $SrAl_2O_4$ material as the host lattice absorbs the soft X-ray photon energy and stores it in electron traps. Then, the energy gets away from the electron traps and transfers to the $4f^65d^1$ energy level in the $Eu^{2+}$ ion, which causes the $Eu^{2+}$ ion to produce radioactive transition luminescence.

### 2. 1. 4 $B^{3+}$-doped PLMs

$B^{3+}$ ion can replace $Ga^{3+}$ ion in $ZnGa_2O_4$ materials to improve the optical performance of $ZnGa_2O_4$ materials because of the similarity of valence and chemical properties between $Ga^{3+}$ and $B^{3+}$ ions. Wang et al. researched the changes in the optical performance of $ZnGa_2O_4$ materials after $B^{3+}$-doping[18]. Both $ZnGa_2O_4$ and $ZnGa_2O_4$:$B^{3+}$ can

detect phosphorescence signal peaks at 502 and 695 nm. However, the phosphorescence decay curves indicate that the phosphorescence intensity and the phosphorescence time of $ZnGa_2O_4:B^{3+}$ have been significantly improved compared with $ZnGa_2O_4$. According to previous reports, the proper trap depth is essential to achieve a better optical performance of PLMs[1, 47, 48]. There is a bold inference that the introduction of $B^{3+}$ ion can also increase the content of electron traps $Ga_{Zn}^{\cdot}$, thus leading to the enhancement of optical performance of $ZnGa_2O_4$ after $B^{3+}$-doping.

## 2. 2 Influence of the number of types of doped ions on the structure and optical performance of PLMs

As above mentioned, the structure and optical performance of PLMs are closely related to the type of doped ions. Most PLMs used in practical applications need to be doped with multiple ions to enhance optical performance. The simultaneous introduction of multiple ions will affect not only the host of PLMs, but also the interaction among different ions. Therefore, we introduce the influence of the number of types of doped ions on the structure and optical performance of PLMs in this section.

### 2. 2. 1 $Ge^{4+}$ and $Cr^{3+}$ co-doped PLMs

The introduction of $Ge^{4+}$ ion will change the width of the material bandgap due to its unique electronic structure. Thus, the change of structure and optical performance of $Ge^{4+}$, $Cr^{3+}$ co-doped PLMs is discussed[5]. Wang et al. found that the crystal phases of the $Cr^{3+}$-doped $ZnGa_{1.995}O_4$ and $Ge^{4+}$, $Cr^{3+}$ co-doped $ZnGa_{1.995}O_4$ materials are corresponding to the standard pattern, indicating that the structure of the materials has not obviously changed after $Ge^{4+}$, $Cr^{3+}$ co-doping. In addition, the emission spectra of $ZnGa_{1.995}O_4:Cr^{3+}$ and $Zn_{1.25}Ga_{1.5}Ge_{0.25}O_4:Cr^{3+}$ both present a near-infrared emission band of 650～900 nm[49, 50]. The phosphorescence decay curves show that the optical performance of $Zn_{1.25}Ga_{1.5}Ge_{0.25}O_4:Cr^{3+}$ is better than that of $ZnGa_{1.995}O_4:Cr^{3+}$[5]. Based on the above results, the introduction of $Ge^{4+}$ improves the filling efficiency of electron traps, thus increasing the phosphorescence time of the materials[23].

### 2. 2. 2 $Pr^{3+}$, $Cr^{3+}$ co-doped PLMs

The number and depth of the trap energy levels of PLMs are changed after the introduction of $Pr^{3+}$ ion because of the special 4*f*5*d* electronic structure and abundant electronic transition types of $Pr^{3+}$ ion. Therefore, the changes in structure and optical performance of $Zn_{2.94}Ga_{1.96}Ge_2O_{10}$ after the introduction of $Pr^{3+}$ and $Cr^{3+}$ ions are discussed[19]. By analyzing the XRD pattern, the structure of $Zn_{2.94}Ga_{1.96}Ge_2O_{10}:Cr^{3+}$, $Pr^{3+}$ has not obviously changed, and the pure spinel phase is still maintained. Later, the author does in-depth studies on the optical performance of $Zn_{2.94}Ga_{1.96}Ge_2O_{10}:Pr^{3+}$, $Cr^{3+}$. The electrons recombine with holes in the natural defects, thereby leading to a wide emission band of 350～660 nm. In addition, the $Cr^{3+}$ ion provides a near-infrared emission band of 695 nm through the $^2E \rightarrow {}^4A_2$ transition[27], while the $Pr^{3+}$ ion increases the phosphorescence time by adjusting the depth and density of traps based on the energy levels of 4*f* electron configurations[51-55]. Similarly, Yu et al. did further research on the persistent luminescence mechanisms of $Zn_3Ga_2GeO_8:Cr^{3+}$, $Pr^{3+}$ to clarify the function of $Pr^{3+}$ ion[56]. The introduction of $Pr^{3+}$ ion deepens the trap energy level and increases the number of traps. Given this, a possible persistent luminescence mechanism of $Zn_3Ga_2GeO_8:Cr^{3+}$, $Pr^{3+}$ is proposed (Fig. 3). Trap *A* forms more traps than trap *A*′ by introducing $Pr^{3+}$ ion, thereby improving the phosphorescence intensity and the phosphorescence time of $Zn_3Ga_2GeO_8:Cr^{3+}$, $Pr^{3+}$ materials.

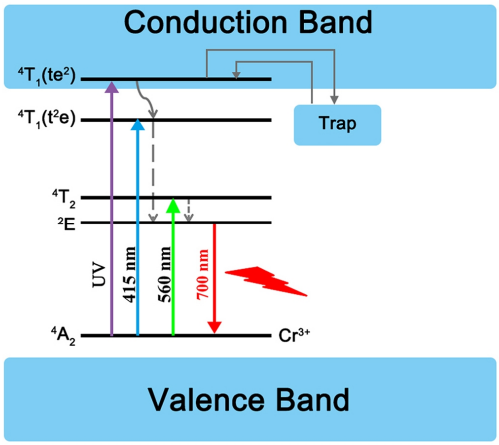


**Fig. 3. Persistent luminescence mechanism of $Zn_{2.94}Ga_{1.96}Ge_2O_{10}:Pr^{3+}$, $Cr^{3+}$ materials**

### 2. 2. 3 $Yb^{3+}$, $Er^{3+}$, $Cr^{3+}$ co-doped PLMs

$Yb^{3+}$ ion and $Er^{3+}$ ion are rare earth element ions used as luminescence centers, which are usually introduced into PLMs to change the density and depth of the trap levels resulting from their unique electronic structure. Consequently, the structure and optical performance of $Zn_{1.25}Ga_{1.5}Ge_{0.25}O_4$:$Yb^{3+}$, $Er^{3+}$, $Cr^{3+}$ (ZGGO:$Cr^{3+}$, $Yb^{3+}$, $Er^{3+}$) with a pure spinel phase is discussed[23]. Yan et al. found that the structure of $Zn_{1.25}Ga_{1.5}Ge_{0.25}O_4$ has not obviously changed after doping with $Yb^{3+}$, $Er^{3+}$ and $Cr^{3+}$ ion. Moreover, ZGGO:$Cr^{3+}$, $Yb^{3+}$, $Er^3$ presents an excellent optical performance, and the phosphorescence time exceeds 20 days. Later, the author studied the persistent luminescence mechanism of ZGGO:$Yb^{3+}$, $Er^{3+}$, $Cr^{3+}$ (Fig. 4). The excited electrons are captured by electron traps under ultraviolet light irradiation, and then moves to deep traps by means of nonradiative relaxation. Subsequently, the combination of the excited electrons and the $Cr^{3+}$ ion leads to the formation of a persistent phosphorescence signal after the ultraviolet radiation is stopped. The introduction of $Yb^{3+}$ and $Er^{3+}$ ions can not only provide the materials with additional electrons and energy levels, but also adjust the density and depth of traps[51, 57, 58]. The excited electrons are trapped in the deepest 4*f* energy levels of $Yb^{3+}$ and $Er^{3+}$ ions, thereby extending the time for the trapped electrons to return to the $^2E$ energy level of $Cr^{3+}$ ion (Fig. 4a, b)[58], which also obviously prolongs the phosphorescence time of materials.

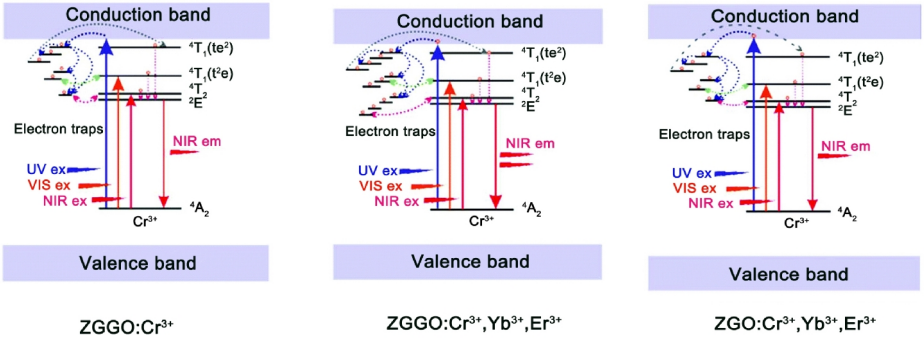


**(a) (b) (c)**

**Fig. 4. Persistent luminescence mechanism of (a) ZGGO:$Cr^{3+}$, (b) ZGGO:$Cr^{3+}$,$Yb^{3+}$,$Er^{3+}$, (c) ZGO:$Cr^{3+}$,$Yb^{3+}$,$Er^{3+}$. ZGO refers to a zinc gallate matrix**

### 2. 2. 4 $Eu^{3+}$, $Ti^{4+}$ and $Mg^{2+}$ co-doped PLMs

Viana et al. researched the structure and optical performance of $Eu^{3+}$, $Ti^{4+}$, $Mg^{2+}$ co-doped $Gd_2O_2S$ materials with a pure hexagonal $Gd_2O_2S$ phase[20]. The study found that $Ti^{4+}$ and $Mg^{2+}$ ions are trapping centers, and $Eu^{3+}$ ions are the emission centers. The $Gd_2O_2S$:$Eu^{3+}$, $Ti^{4+}$, $Mg^{2+}$ has an emission band of 580～720 nm due to the electronic transitions of $Eu^{3+}$ ion. Therefore, it can be inferred that the $Eu^{3+}$ ion plays the role of the luminescence center in the materials. Moreover, $Gd_2O_2S$: $Eu^{3+}$, $Ti^{4+}$, $Mg^{2+}$ has a longer phosphorescence time compared with $Gd_2O_2S$: $Eu^{3+}$ for the reason that $Ti^{4+}$ and $Mg^{2+}$ ions play an important in improving the density of trap energy levels. However, the particle size and crystal structure of $Gd_2O_2S$ materials have not obviously changed after the introduction of $Eu^{3+}$, $Ti^{4+}$ and $Mg^{2+}$ ions.

## 2. 3 Influence of the content of doped ions on the structure and optical performance of PLMs

As mentioned above, some doped ions play the role of the emission center of PLMs, while other doped ions will affect the number and depth of trap levels. Therefore, it is of great necessity to understand how the content of doped ions influences the structure and optical performance of PLMs. This section will discuss how the content of doped ions affects the structure and optical performance of PLMs.

### 2. 3. 1 $Pr^{3+}$, $Cr^{3+}$ co-doped PLMs

Normally, $Cr^{3+}$ ion serves as the luminescence center of PLMs, while $Pr^{3+}$ ion affects the number and depth of trap levels. Yan et al. studied how the contents of $Pr^{3+}$ and $Cr^{3+}$ ions influence the structure and optical performance of PLMs. It is found that the increase of $Cr^{3+}$ content promotes the energy release of $Zn_{2.94}Ga_{1.96}Ge_2O_{10}$:$Cr^{3+}$, $Pr^{3+}$. Therefore, as the amount of $Cr^{3+}$ ion doping increases, the phosphorescence intensity and phosphorescence time of the material decrease[19, 27, 59]. Similarly, Zhang et al. studied the changes in particle size of $Pr^{3+}$, $Cr^{3+}$ co-doped $Zn_2Ga_{2.98-x}Ge_{0.75}O_8$

materials with different $Pr^{3+}$ contents[22]. It is found that the average size of the materials decreases with the increase of $Pr^{3+}$ contents. Considering that the doped ions can strongly affect the crystal growth rate through surface charge modification[60], the size reduction of $Zn_2Ga_{2.98-x}Ge_{0.75}O_8$:$Cr^{3+}$, $Pr^{3+}$ may be related to the influence of $Pr^{3+}$ ion on the surface charge of the material. Specifically, the surface charge distribution of the materials will be changed when the $Pr^{3+}$ ion is introduced into the materials, thereby reducing the growth rate. Subsequently, the optical performance of $Pr^{3+}$, $Cr^{3+}$ co-doped $Zn_2Ga_{2.98-x}Ge_{0.75}O_8$ materials is researched. As shown in Fig. 5a, the phosphorescence intensity and the phosphorescence time of the materials increase as the increase of $Pr^{3+}$ doping contents due to the changes in the trap levels of the materials caused by the introduction of $Pr^{3+}$ ion (Fig. 5b). When the content of $Pr^{3+}$ ion is too high, the luminescence performance will decrease due to the concentration quenching effect.

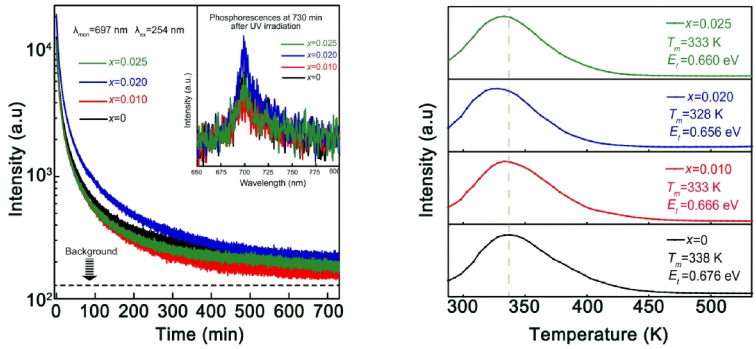


**(a)** **(b)**

**Fig. 5. (a) Phosphorescence decay curves of $Pr^{3+}$, $Cr^{3+}$ co-doped $Zn_2Ga_{2.98-x}Ge_{0.75}O_8$ materials with different $Pr^{3+}$ doping contents. The inset presents the phosphorescence intensity of the materials after the ultraviolet light irradiation is stopped, (b) Thermo-luminescence spectra of $Pr^{3+}$, $Cr^{3+}$ co-doped $Zn_2Ga_{2.98-x}Ge_{0.75}O_8$ materials with different $Pr^{3+}$ doping contents**

### 2. 3. 2 $Bi^{3+}$, $Cr^{3+}$ co-doped PLMs

$Bi^{3+}$ ion can significantly reduce the bandgap energy of PLMs and improve the efficiency of electron trap filling resulting from its unique 6*s* orbital. Tuerdi et al. researched the influence of crystalline structure, emission peak wavelength and phosphorescence time of $ZnGa_2O_4$:$Bi^{3+}$, $Cr^{3+}$ materials with different $Bi^{3+}$ doping contents[16]. The $Bi^{3+}$ ion tends to replace $Ga^{3+}$ ion in $ZnGa_2O_4$ with a similar ion radius, which makes the material produce higher periodic lattice distortion, thereby making the materials exhibit a longer phosphorescence time. When the doped ratio of $Bi^{3+}$ ion is low, the crystal phase of $Cr^{3+}$, $Bi^{3+}$ co-doped $ZnGa_2O_4$ materials corresponds to its standard spectrum, indicating that the structure of $ZnGa_2O_4$ materials has not obviously changed after the introduction of $Bi^{3+}$ ion. However, when the doped ratio of $Bi^{3+}$ ion increases to 0.03, a strong peak related to the rhombohedral $Bi^{3+}$ structure at 28.01° is observed in the XRD pattern (Fig. 6a), illustrating that the original crystal structure of the materials is destroyed. Correspondingly, its optical performance is also reduced. The phosphorescence emission spectrum of $ZnGa_2O_4$:$Bi^{3+}$, $Cr^{3+}$ materials with different $Bi^{3+}$ doping contents shows a red-shift of emission peak wavelength, which indicates that $Bi^{3+}$ ion reduces the crystal field intensity of the $Cr^{3+}$ ion (Fig. 6b).

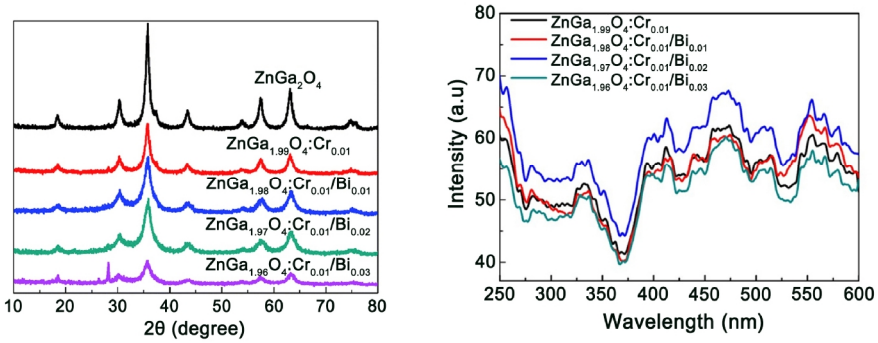


**(a)** **(b)**

**Fig. 6. (a) XRD patterns of $ZnGa_2O_4$, $ZnGa_2O_4$:$Cr^{3+}$ and $ZnGa_2O_4$:$Cr^{3+}$, $Bi^{3+}$, (b) Phosphorescence spectra of $ZnGa_2O_4$, $ZnGa_2O_4$:$Cr^{3+}$ and $ZnGa_2O_4$:$Cr^{3+}$, $Bi^{3+}$**

### 2. 3. 3 $B^{3+}$, $Cr^{3+}$ co-doped PLMs

As mentioned above, the introduction of $B^{3+}$ ion can improve the optical performance of $ZnGa_2O_4$. On this basis, the researchers studied the influence of doped ion content on PLMs. For example, Yan et al. synthesized $ZnGa_2O_4:B^{3+}$, $Cr^{3+}$ materials by hydrothermal method, and studied the optical performance of $ZnGa_2O_4:Cr^{3+}$ with different $B^{3+}$ doping contents[17]. The XRD pattern presents that the structure of the material has not obviously changed after doping with the $B^{3+}$ and $Cr^{3+}$ ions. Besides, the emission wavelength of the materials has not obviously changed when the $B^{3+}$ ion is introduced into the materials, which indicates that the $B^{3+}$ ion does not play the role of luminescence center in the materials. At the same time, the improvement of the optical performance of materials shows that the introduction of $B^{3+}$ ion injects new electron traps into the materials and increases the content of electron traps.

### 2. 3. 4 $Eu^{3+}$, $Ti^{4+}$ and $Mg^{2+}$ co-doped PLMs

$Eu^{3+}$, $Ti^{4+}$ and $Mg^{2+}$ ions will act as luminescence centers or trap levels to affect the optical performance of the material. Therefore, studying the optical performance of $Gd_2O_2S:Eu^{3+}$, $Ti^{4+}$ and $Mg^{2+}$ materials with different doping contents will help us better understand the role of these ions in the material[20]. The study found that $Eu^{3+}$ ion provides trap levels for electron-hole recombination, and $Ti^{4+}$ ion provides electron traps to achieve the formation of the phosphorescence signal. Since $Ti^{4+}$ ion replaces $Gd^{3+}$ ion and destroys the charge conservation of the materials, it is necessary to introduce $Mg^{2+}$ ion to maintain charge balance. In addition, as the doping contents of $Mg^{2+}$ ion increase, the phosphorescence intensity of the material increases. This indicates that the introduction of $Mg^{2+}$ ion can induce the formation of intermediate trap levels in the material, which prolongs the storage time of the carriers in the material, thus realizing the improvement of the persistent performance of the materials[61].

Apart from the ion-doped PLMs mentioned above, other doped ions also have an impact on the structure and optical performance. For example, $Li_2ZnGeO_4:Mn^{2+}$[62], $SrAl_2O_4:Eu^{2+}$, $Dy^{3+}$[63], $GdAlO_3:Mn^{4+}$, $Ge^{4+}$[64], $LaAlO_3:Mn^{4+}$, $Ge^{4+}$[65], $CaMgSi_2O_6:Eu^{2+}$, $Dy^{3+}$, $Mn^{2+}$[66], $Y_3Al_{5-x}Ga_xO_{12}:Ce^{3+}$, $Bi^{3+}$ ($x$ = 0 ～ 4)[67], $MgGeO_3:Mn^{2+}$, $Bi^{3+}$[68], $Y_3Sc_2Ga_3O_{12}:Ce^{3+}$[69], $Ca_9Bi(PO_4)_7:Ce^{3+}$, $Tb^{3+}$, $Mn^{2+}$[70], $Ca_2BO_3Cl:Eu^{2+}$, $Dy^{3+}$[71], $Lu_2O_3:Tb^{3+}$, $Ca^{2+}$[72], $KY_3F_{10}:Tb^{3+}$[73] and $AlN:Mn^{2+}$[74].

## 3 CONCLUSION

In this review, we mainly focus on the impact of the type of doped ions, the number of types of doped ions, and the content of doped ions on the structure and optical performance of PLMs. In the past decade, although various doped ions have been widely used to improve the optical performance of PLMs, there is still much work to do in the future. First, in the actual preparation process, the optical performance of PLMs will be affected by the symmetry of matrix lattice, the radius of activated ions, and the electronegativity and distribution of external electron cloud. This should be paid more attention to by researchers. Second, exploring the relationship between doped ions and the host lattice and investigating the influence of the defects caused by doped ions on the storage time of the carriers. At present, these issues still have no exact quantitative relationship, and further researches are needed. Third, understanding the role of trap types, trap contents and probability of trapping electrons in the researches of the persistent luminescence mechanisms. Forth, exploring new doped ions and substrates. For example, most current PLMs are based on aluminates, gallates and silicates matrices. It is necessary to find new matrices with excellent properties. Collectively, with the deepening research of PLMs, ion-doped PLMs with higher luminescence intensity and phosphorescence lifetime will have a broad development prospect.

## REFERENCES

(1) Van den Eeckhout, K.; Smet, P. F.; Poelman, D. Persistent luminescence in $Eu^{2+}$-doped compounds: a review. *Materials* **2010**, 3, 2536- 2566.

(2) Zhou, Z.; Zheng, W.; Kong, J.; Liu, Y.; Huang, P.; Zhou, S.; Chen, Z.; Shi, J.; Chen, X. Rechargeable and LED-activated $ZnGa_2O_4:Cr^{3+}$ near-infrared persistent luminescence nanoprobes for background-free biodetection. *Nanoscale* **2017**, 9, 6846- 6853.

(3) Song, L.; Li, P. P.; Yang, W.; Lin, X. H.; Liang, H.; Chen, X. F.; Liu, G.; Li, J.; Yang, H. H. Low-dose X-ray activation of W(VI)-doped persistent luminescence nanoparticles for deep-tissue photodynamic therapy. *Adv. Funct. Mater.* **2018**, 28, 1707496- 10.

(4) Song, L.; Lin, X. H.; Song, X. R.; Chen, S.; Chen, X. F.; Li, J.; Yang, H. H. Repeatable deep-tissue activation of persistent luminescent nanoparticles by soft X-ray for high sensitivity long-term in vivo bioimaging. *Nanoscale* **2017**, 9, 2718- 2722

(5) Liu, Y.; Liu, J. M.; Zhang, D.; Ge, K.; Wang, P.; Liu, H.; Fang, G.; Wang, S. Persistent luminescence nanophosphor involved near-infrared optical bioimaging for investigation of foodborne probiotics biodistribution in vivo: a proof-of-concept study. *J. Agric. Food. Chem.* **2017**, 65, 8229- 8240.

(6) Xue, Z.; Li, X.; Li, Y.; Jiang, M.; Liu, H.; Zeng, S.; Hao, J. X-ray-activated near-infrared persistent luminescent probe for deep-tissue and renewable in vivo bioimaging. *ACS Appl. Mater. Inter.* **2017**, 9, 22132- 22142.

(7) Lv, Y.; Ding, D.; Zhuang, Y.; Feng, Y.; Shi, J.; Zhang, H.; Zhou, T. L.; Chen, H.; Xie, R. J. Chromium-doped zinc gallogermanate@zeolitic imidazolate framework-8: a multifunctional nanoplatform for rechargeable in vivo persistent luminescence imaging and pH-responsive drug release. *ACS Appl. Mater. Inter.* **2019**, 11, 1907- 1916.

(8) Li, Y.; Gecevicius, M.; Qiu, J. Long persistent phosphors-from fundamentals to applications. *Chem. Soc. Rev.* **2016**, 45, 2090- 2136.

(9) Chander, H.; Haranath, D.; Shanker, V.; Sharma, P. Synthesis of nanocrystals of long persisting phosphor by modified combustion technique. *J. Cryst. Growth* **2004**, 271, 307- 312.

(10) Lecuyer, T.; Teston, E.; Ramirez Garcia, G.; Maldiney, T.; Viana, B.; Seguin, J.; Mignet, N.; Scherman, D.; Richard, C. Chemically engineered persistent luminescence nanoprobes for bioimaging. *Theranostics* **2016**, 6, 2488- 2524.

(11) Yamamoto, H.; Matsuzawa, T. Mechanism of long phosphorescence of $SrAl_2O_4$:$Eu^{2+}$, $Dy^{3+}$ and $CaAl_2O_4$:$Eu^{2+}$, $Nd^{3+}$. *J. Lumin.* **1997**, 72- 74, 287- 289.

(12) Zhuang, Y.; Lv, Y.; Wang, L.; Chen, W.; Zhou, T. L.; Takeda, T.; Hirosaki, N.; Xie, R. J. Trap depth engineering of $SrSi_2O_2N_2$:$Ln^{2+}$,$Ln^{3+}$ ($Ln^{2+}$ = Yb, Eu; $Ln^{3+}$ = Dy, Ho, Er) persistent luminescence materials for information storage applications. *ACS Appl. Mater. Inter.* **2018**, 10, 1854- 1864.

(13) Cui, G.; Yang, X.; Zhang, Y.; Fan, Y.; Chen, P.; Cui, H.; Liu, Y.; Shi, X.; Shang, Q.; Tang, B. Round-the-clock photocatalytic hydrogen production with high efficiency by a long-afterglow material. *Angew. Chem. Int. Ed.* **2019**, 58, 1340- 1344.

(14) Liu, J.; Lecuyer, T.; Seguin, J.; Mignet, N.; Scherman, D.; Viana, B.; Richard, C. Imaging and therapeutic applications of persistent luminescence nanomaterials. *Adv. Drug Deliver. Rev.* **2019**, 138, 193- 210.

(15) Luo, Q.; Wang, W.; Tan, J.; Yuan, Q. Surface modified persistent luminescence probes for biosensing and bioimaging: a review. *Chin. J. Chem.* **2021**, 39, 1009- 1021.

(16) Tuerdi, A.; Abdukayum, A. Dual-functional persistent luminescent nanoparticles with enhanced persistent luminescence and photocatalytic activity. *RSC Adv.* **2019**, 9, 17653- 17657.

(17) Zhao, H. X.; Yang, C. X.; Yan, X. P. Fabrication and bioconjugation of B(III) and Cr(III) co-doped $ZnGa_2O_4$ persistent luminescent nanoparticles for dual-targeted cancer bioimaging. *Nanoscale* **2016**, 8, 18987- 18994.

(18) Li, D.; Wang, Y.; Xu, K.; Zhao, H.; Hu, Z. Effect of $H_3BO_3$ on the persistent luminescence and photocatalytic properties of $ZnGa_2O_4$ phosphors. *Opt. Mater.* **2014**, 36, 1836- 1840.

(19) Abdukayum, A.; Chen, J. T.; Zhao, Q.; Yan, X. P. Functional near infrared-emitting $Cr^{3+}$/$Pr^{3+}$ co-doped zinc gallogermanate persistent luminescent nanoparticles with superlong afterglow for in vivo targeted bioimaging. *J. Am. Chem. Soc.* **2013**, 135, 14125- 14133.

(20) Rosticher, C.; Viana, B.; Fortin, M. A.; Lagueux, J.; Faucher, L.; Chanéac, C. Gadolinium oxysulfide nanoprobes with both persistent luminescent and magnetic properties for multimodal imaging. *RSC Adv.* **2016**, 6, 55472- 55478.

(21) Wang, J.; Ma, Q.; Zheng, W.; Liu, H.; Yin, C.; Wang, F.; Chen, X.; Yuan, Q.; Tan, W. One-dimensional luminous nanorods featuring tunable persistent luminescence for autofluorescence-free biosensing. *ACS Nano* 2017, 11, 8185- 8191.

(22) Gong, Z.; Liu, Y.; Yang, J.; Yan, D.; Zhu, H.; Liu, C.; Xu, C.; Zhang, H. A $Pr^{3+}$ doping strategy for simultaneously optimizing the size and near infrared persistent luminescence of ZGGO:Cr(3+) nanoparticles for potential bio-imaging. *Phys. Chem. Chem. Phys.* **2017**, 19, 24513- 24521.

(23) Li, Y. J.; Yan, X. P. Synthesis of functionalized triple-doped zinc gallogermanate nanoparticles with superlong near-infrared persistent luminescence for long-term orally administrated bioimaging. *Nanoscale* **2016**, 8, 14965- 14970.

(24) Jiang, R.; Yang, J.; Meng, Y.; Yan, D.; Liu, C.; Xu, C.; Liu, Y. X-ray/red-light excited ZGGO:Cr,Nd nanoprobes for NIR-I/II afterglow imaging. *Dalton T.* **2020**, 49, 6074- 6083.

(25) Wang, J.; Ma, Q.; Wang, Y.; Shen, H.; Yuan, Q. Recent progress in biomedical applications of persistent luminescence nanoparticles. *Nanoscale* **2017**, 9, 6204- 6218.

(26) Singh, S. K. Red and near infrared persistent luminescence nano-probes for bioimaging and targeting applications. *RSC Adv.* **2014**, 4, 58674- 58698.

(27) Bessière, A.; Jacquart, S.; Priolkar, K.; Lecointre, A.; Viana, B.; Gourier, D. $ZnGa_2O_4$:$Cr^{3+}$: a new red long-lasting phosphor with high brightness. *Opt. Express* **2011**, 19, 10131- 10137.

(28) Allix, M.; Chenu, S.; Véron, E.; Poumeyrol, T.; Kouadri Boudjelthia, E. A.; Alahraché, S.; Porcher, F.; Massiot, D.; Fayon, F. Considerable improvement of long-persistent luminescence in germanium and tin substituted $ZnGa_2O_4$. *Chem. Mater.* **2013**, 25, 1600- 1606.

(29) Dhak, P.; Gayen, U. K.; Mishra, S.; Pramanik, P.; Roy, A. Optical emission spectra of chromium doped nanocrystalline zinc gallate. *J. Appl. Phys.* **2009**, 106, 063721- 6.

(30) Kim, J. S.; Kim, J. S.; Park, H. L. Optical and structural properties of nanosized $ZnGa_2O_4:Cr^{3+}$ phosphor. *Solid State Commun.* **2004**, 131, 735- 738.

(31) Xu, J.; Murata, D.; Ueda, J.; Viana, B.; Tanabe, S. Toward rechargeable persistent luminescence for the first and third biological windows via persistent energy transfer and electron trap redistribution. *Inorg. Chem.* **2018**, 57, 5194- 5203.

(32) Feng, P.; Li, G.; Guo, H.; Liu, D.; Ye, Q.; Wang, Y. Identifying a cyan ultralong persistent phosphorescence (Ba, Li) (Si, Ge, P)$_2O_5:Eu^{2+}$, $Pr^{3+}$ via solid solution strategy. *J. Phys. Chem. C* **2019**, 123, 3102- 3109.

(33) Bai, Q.; Zhao, S.; Guan, L.; Wang, Z.; Li, P.; Xu, Z. Design and control of the luminescence of $Cr^{3+}$-doped phosphors in the near-infrared I region by fitting the crystal field. *Cryst. Growth Des.* **2018**, 18, 3178- 3186.

(34) Takahashi, Y.; Ando, M.; Ihara, R.; Fujiwara, T. Green-emissive Mn-activated nanocrystallized glass with willemite-type $Zn_2GeO_4$. *Opt. Mater. Express* **2011**, 1, 372- 378.

(35) Terraschke, H.; Wickleder, C. UV, blue, green, yellow, red, and small: newest developments on $Eu^{2+}$-doped nanophosphors. *Chem. Rev.* **2015**, 115, 11352- 11378.

(36) Cheng, J.; Li, P.; Wang, Z.; Li, Z.; Tian, M.; Wang, C.; Yang, Z. Color selective manipulation in $Li_2ZnGe_3O_8:Mn^{2+}$ by multiple-cation substitution on different crystal-sites. *Dalton T.* **2018**, 47, 4293- 4300.

(37) Li, Z.; Wang, Q.; Wang, Y.; Ma, Q.; Wang, J.; Li, Z.; Li, Y.; Lv, X.; Wei, W.; Chen, L.; Yuan, Q. Background-free latent fingerprint imaging based on nanocrystals with long-lived luminescence and pH-guided recognition. *Nano Res.* **2018**, 11, 6167- 6176.

(38) Feng, Y.; Deng, D.; Zhang, L.; Liu, R.; Lv, Y. LRET-based functional persistent luminescence nanoprobe for imaging and detection of cyanide ion. *Sens. Actuators B-Chem.* **2019**, 279, 189- 196.

(39) Wang, J.; Ma, Q.; Wang, Y.; Li, Z.; Li, Z.; Yuan, Q. New insights into the structure-performance relationships of mesoporous materials in analytical science. *Chem. Soc. Rev.* **2018**, 47, 8766- 8803.

(40) Liu, H.; Hu, X.; Wang, J.; Liu, M.; Wei, W.; Yuan, Q. Direct low-temperature synthesis of ultralong persistent luminescence nanobelts based on a biphasic solution-chemical reaction. *Chin. Chem. Lett.* **2018**, 29, 1641- 1644.

(41) Wang, Y.; Wang, J.; Ma, Q.; Li, Z.; Yuan, Q. Recent progress in background-free latent fingerprint imaging. *Nano Res.* **2018**, 11, 5499- 5518.

(42) Cheng, S.; Shen, B.; Yuan, W.; Zhou, X.; Liu, Q.; Kong, M.; Shi, Y.; Yang, P.; Feng, W.; Li, F. Time-gated ratiometric detection with the same working wavelength to minimize the interferences from photon attenuation for accurate in vivo detection. *ACS Cent. Sci.* **2019**, 5, 299- 307.

(43) Ou, X. Y.; Guo, T.; Song, L.; Liang, H. Y.; Zhang, Q. Z.; Liao, J. Q.; Li, J. Y.; Li, J.; Yang, H. H. Autofluorescence-free immunoassay using X-ray scintillating nanotags. *Anal. Chem.* **2018**, 90, 6992- 6997.

(44) Wang, J.; Ma, Q.; Liu, H.; Wang, Y.; Shen, H.; Hu, X.; Ma, C.; Yuan, Q.; Tan, W. Time-gated imaging of latent fingerprints and specific visualization of protein secretions via molecular recognition. *Anal. Chem.* **2017**, 89, 12764- 12770.

(45) Shen, H.; Wang, Y.; Wang, J.; Li, Z.; Yuan, Q. Emerging biomimetic applications of DNA nanotechnology. *ACS Appl. Mater. Inter.* **2019**, 11, 13859- 13873.

(46) Jia, D.; Jia, W.; Evans, D. R.; Dennis, W. M.; Liu, H.; Zhu, J.; Yen, W. M. Trapping processes in $CaS:Eu^{2+},Tm^{3+}$. *J. Appl. Phys.* **2000**, 88, 3402- 3407.

(47) Guo, C.; Tang, Q.; Huang, D.; Zhang, C.; Su, Q. Tunable color emission and afterglow in $CaGa_2S_4:Eu^{2+}$, $Ho^{3+}$ phosphor. *Mater. Res. Bull.* **2007**, 42, 2032- 2039.

(48) Denis, G.; Deniard, P.; Rocquefelte, X.; Benabdesselam, M.; Jobic, S. The thermally connected traps model applied to the thermoluminescence of $Eu^{2+}$ doped $Ba_{13-x}Al_{22-2x}Si_{10+2x}O_{66}$ materials ($x\sim0.6$). *Opt. Mater.* **2010**, 32, 941- 945.

(49) Struve, B.; Huber, G. The effect of the crystal field strength on the optical spectra of $Cr^{3+}$ in gallium garnet laser crystals. *Appl. Phys. B* **1985**, 36, 195- 201.

(50) Forster, L. S. The photophysics of chromium(III) complexes. *Chem. Rev.* **1990**, 90, 331- 353.

(51) Maldiney, T.; Lecointre, A.; Viana, B.; Bessiere, A.; Bessodes, M.; Gourier, D.; Richard, C.; Scherman, D. Controlling electron trap depth to enhance optical properties of persistent luminescence nanoparticles for in vivo imaging. *J. Am. Chem. Soc.* **2011**, 133, 11810- 11815.

(52) Jia, G.; Lewis, L.; Wang, X. Cr(3+)-doped lanthanum gallogermanate phosphors with long persistent IR emission. *Electrochem. Solid St.* **2010**, 13, J32- J34.

(53) Aitasalo, T.; Dereń, P.; Hölsä, J.; Jungner, H.; Krupa, J. C.; Lastusaari, M.; Legendziewicz, J.; Niittykoski, J.; Stręk, W. Persistent luminescence phenomena in materials doped with rare earth ions. *J. Solid State Chem.* **2003**, 171, 114- 122.

(54) Li, X.; Zhang, F.; Zhao, D. Highly efficient lanthanide upconverting nanomaterials: progresses and challenges. *Nano Today* **2013**, 8, 643- 676.

(55) Dong, H.; Sun, L. D.; Yan, C. H. Basic understanding of the lanthanide related upconversion emissions. *Nanoscale* **2013**, 5, 5703- 5714.

(56) Cai, Y.; Liu, B.; Chen, W.; Qiu, J.; Xu, X.; Zhao, L.; Yu, X. X-ray and UV excited long persistent luminescence properties of $Zn_3Ga_2GeO_8$: $Cr^{3+}$, $Pr^{3+}$. *ECS J. Solid State Sc.* **2020**, 9, 066006- 7.

(57) Sun, S. K.; Wang, H. F.; Yan, X. P. Engineering persistent luminescence nanoparticles for biological applications: from biosensing/bioimaging to theranostics. *Acc. Chem. Res.* **2018**, 51, 1131- 1143.

(58) Qu, B.; Zhang, B.; Wang, L.; Zhou, R.; Zeng, X. C. Mechanistic study of the persistent luminescence of $CaAl_2O_4$:Eu,Nd. *Chem. Mater.* **2015**, 27, 2195- 2202.

(59) Pan, Z.; Lu, Y. Y.; Liu, F. Sunlight-activated long-persistent luminescence in the near-infrared from $Cr^{3+}$-doped zinc gallogermanates. *Nat. Mater.* **2011**, 11, 58- 63.

(60) Wang, F.; Han, Y.; Lim, C. S.; Lu, Y.; Wang, J.; Xu, J.; Chen, H.; Zhang, C.; Hong, M.; Liu, X. Simultaneous phase and size control of upconversion nanocrystals through lanthanide doping. *Nature* **2010**, 463, 1061- 1065.

(61) Mikami, M.; Oshiyama, A. First-principles study of intrinsic defects in yttrium oxysulfide. *Phys. Rev. B* **1999**, 60, 1707- 1715.

(62) Li, P.; Peng, M.; Wondraczek, L.; Zhao, Y.; Viana, B. Red to near infrared ultralong lasting luminescence from $Mn^{2+}$-doped sodium gallium aluminum germanate glasses and (Al,Ga)-albite glass-ceramics. *J. Mater. Chem. C* **2015**, 3, 3406- 3415.

(63) Kandpal, S. K.; Goundie, B.; Wright, J.; Pollock, R. A.; Mason, M. D.; Meulenberg, R. W. Investigation of the emission mechanism in milled $SrAl_2O_4$:Eu, Dy using optical and synchrotron X-ray spectroscopy. *ACS Appl. Mater. Inter.* **2011**, 3, 3482- 3486.

(64) Liu, J. M.; Liu, Y. Y.; Zhang, D. D.; Fang, G. Z.; Wang, S. Synthesis of $GdAlO_3$:$Mn^{4+}$,$Ge^{4+}$@Au core-shell nanoprobes with plasmon-enhanced near-infrared persistent luminescence for in vivo trimodality bioimaging. *ACS Appl. Mater. Inter.* **2016**, 8, 29939- 29949.

(65) Li, Y.; Li, Y. Y.; Sharafudeen, K.; Dong, G. P.; Zhou, S. F.; Ma, Z. J.; Peng, M. Y.; Qiu, J. R. A strategy for developing near infrared long-persistent phosphors: taking $MAlO_3$:$Mn^{4+}$,$Ge^{4+}$ (M = La, Gd) as an example. *J. Mater. Chem. C* **2014**, 2, 2019- 2027.

(66) Rosticher, C.; Viana, B.; Laurent, G.; Le Griel, P.; Chanéac, C. Insight into $CaMgSi_2O_6$:$Eu^{2+}$,$Mn^{2+}$,$Dy^{3+}$ nanoprobes: influence of chemical composition and crystallinity on persistent red luminescence. *Eur. J. Inorg. Chem.* **2015**, 3681- 3687.

(67) Katayama, Y.; Hashimoto, A.; Xu, J.; Ueda, J.; Tanabe, S. Thermoluminescence investigation on $Y_3Al_{5-x}Ga_xO_{12}$:$Ce^{3+}$-$Bi^{3+}$ green persistent phosphors. *J. Lumin.* **2017**, 183, 355- 359.

(68) Zhuang, Y.; Katayama, Y.; Ueda, J.; Tanabe, S. A brief review on red to near-infrared persistent luminescence in transition-metal-activated phosphors. *Opt. Mater.* **2014**, 36, 1907- 1912.

(69) Ueda, J.; Aishima, K.; Nishiura, S.; Tanabe, S. Afterglow luminescence in $Ce^{3+}$-doped $Y_3Sc_2Ga_3O_{12}$ ceramics. *Appl. Phys. Express* **2011**, 4, 042602- 3.

(70) Li, K.; Shang, M.; Zhang, Y.; Fan, J.; Lian, H.; Lin, J. Photoluminescence properties of single-component white-emitting $Ca_9Bi(PO_4)_7$:$Ce^{3+}$,$Tb^{3+}$,$Mn^{2+}$ phosphors for UV LEDs. *J. Mater. Chem. C* **2015**, 3, 7096- 7104.

(71) Zeng, W.; Wang, Y.; Han, S.; Chen, W.; Li, G.; Wang, Y.; Wen, Y. Design, synthesis and characterization of a novel yellow long-persistent phosphor: $Ca_2BO_3Cl$:$Eu^{2+}$,$Dy^{3+}$. *J. Mater. Chem. C* **2013**, 1, 3004- 3011.

(72) Trojan Piegza, J.; Niittykoski, J.; Hölsä, J.; Zych, E. Thermoluminescence and kinetics of persistent luminescence of vacuum-sintered $Tb^{3+}$-doped and $Tb^{3+}$,$Ca^{2+}$-codoped $Lu_2O_3$ materials. *Chem. Mater.* **2008**, 20, 2252- 2261.

(73) Cao, C.; Guo, S.; Moon, B. K.; Choi, B. C.; Jeong, J. H. Synthesis, grouping, and optical properties of $REF_3$-KF nanocrystals. *Mater. Chem. Phys.* **2013**, 139, 609- 615.

(74) Zhang, H.; Zheng, M.; Lei, B.; Liu, Y.; Xiao, Y.; Dong, H.; Zhang, Y.; Ye, S. Luminescence properties of red long-lasting phosphorescence phosphor AlN:$Mn^{2+}$. *ECS J. Solid State Sci. Technol.* **2013**, 2, R117- R120.